CHAPTER - 6

Metal-molecule interactions: PATP (p-aminothiophenol) on copper and bismuth based clusters

6.1 Introduction

In the previous chapter, we validated the experimentally observed SERS spectrum of cystine by utilizing DFT calculations, which unveiled the catalytic role of copper nanoparticles in breaking the cystine molecule's disulfide bonds. Similarly, in the present chapter, we employed DFT calculations to validate the experimentally observed SERS spectrum of PATP, a molecule renowned for its fascinating SERS interactions with coinage metals.

In SERS, PATP is an important probe molecule because of its strong interaction with the noble metals. It shows an intense SERS signal and has significance in molecular electronics. Also, the PATP molecule is of interest because it is considered a ‘‘push–pull’’ type molecule containing electron donating and electron accepting groups connected by a conjugated π-system.[1,2] Besides, PATP has been used to prepare surfaces as sensors to study the toxicity levels in human red blood cells.[3] Being an organic pollutant, PATP causes water pollution, denatures proteins and also its direct intake by the human body results in adverse effects.[4]

Therefore, the study of the SERS spectrum of PATP is important for toxicological understanding. For the SERS of PATP (para-aminothiophenol) many studies have been reported where different SERS substrate made up of silver, gold and copper were utilized. Initially it was interpreted that the enhanced Raman signals of PATP, observed in SERS (on noble metal nano-particles) are due to PD (photo-driven) charge transfer.[5–7] Later on it was interpreted with the help of experimental as well as theoretical studies that enhanced Raman signals observed in SERS are not due to PATP but from its dimer, a new surface species, DMAB (p, p’-dimercaptoazobenzene).[8–10] This is responsible for the abnormal SERS spectra of PATP on SERS substrates such as gold, silver, palladium, copper and Au–ZnO nanoparticles.[2,11–14] Further, various theoretical and experimental studies proved that the supposedly observed SERS spectrum of PATP should actually correspond to 4, 4’-dimercaptoazobenzene (DMAB) which is the dimer of PATP, where the b_2 modes of PATP are converted to the a_g modes (at 1140, 1390 and 1432 cm^{-1}) of

DMAB by surface catalytic reaction.[7–9,15–18] The Raman peaks observed at 1390 and 1432 cm^{-1}, assigned to a_g16 and a_g17, respectively, correspond to the –N=N– stretching modes of DMAB.[15] To explain the same Huang et al. carried out SERS study of PATP using gold and silver nanoparticles as a SERS substrate. And they observed the formation of DMAB as a function of the incident laser power during their SERS measurement of PATP.[2,11] Recently, Arathi et al. reported SERS of PATP where the substrate was both bulk copper and copper nano-particles coated on pencil graphite and they too observed the formation of DMAB.[13] They concluded that copper as a substrate behaved similar to silver and gold nanoparticles in acting as a photocatalyst transforming PATP to DMAB.

Measuring the true SERS spectrum of PATP is a challenge although it has been observed under specific experimental conditions and different incident laser powers.[19-20] Similarly, the actual SERS spectra of PATP have also been observed on Pt-based nanostructures.[19] However, since the SERS signals of PATP vary with experimental conditions and with different metal SERS substrates, information of metal–PATP adsorption for genuine SERS spectra is of essential importance to understand the adsorption behavior of PATP.

Recently it was reported that a bismuth based non-noble metal can be utilized as a SERS active substrate for the study of molecular species[20] in lieu of the conventional noble-metal SERS substrates. Furthermore, bismuth-based nanomaterials have the advantages of relatively low cost and high stability and also have unique physical and chemical properties,[21,22] so they can be considered as highly efficient SERS substrates.

According to the literature reported, DFT (Density functional theory) methods have been found to be very efficient in predicting the interaction between adsorbed molecule/moiety and metal surfaces.[23–26] Small-sized copper clusters have been found as efficient model clusters to represent the metal surface for the study of adsorption as shown by Ahmed et al.[27] It is to be noted that the model surface clusters provide an easy extrapolation to the properties of the metal surface.[28] Taking cue from the literature, the molecule–metal cluster model, which has been found very effective for the study of adsorption of respective molecule on the particular metal, has been employed in this work.

Computational validation of DMAB on copper cluster by means of simulated SERS spectrum has not been reported earlier to the best of our knowledge.

Also, the DFT calculations were carried out to understand the surface adsorption of PATP on the β-Bi_2O_3/$Bi_2O_2CO_3$ substrate where the predicted results were found to be in good agreement with experimental observations. Moreover, analysis of the projected density of states also predicted the charge transfer from the molecule to metal, resulting in an enhanced Raman signal of PATP on bismuth based cluster via a chemical enhancement mechanism. For future possibilities, it is envisaged that Bi-based nanoparticles could be exploited for measuring the real SERS spectra of similar compounds like 4-nitrobenzenethiol (4NBT) where photodimerization prevents the SERS measurement of the monomeric compound.

Computational results reported herein substantiated above mentioned experimental results exceedingly well.

6.2 Computational details

For copper surface the Cu5 cluster was utilized since small size metal cluster have been found to be a very efficient model cluster for the study of adsorption.[27,28] Besides, in earlier studies, the predicted results using M5 (M = Ag, Au) cluster have been found in good agreement with the experiment.[9] Therefore in this study the Cu5 metal cluster was utilized throughout the study. The ground state optimization followed by normal modes calculations was carried out for the PATP-Cu5 and Cu5-DMAB-Cu5 systems without having any constraint on the geometry. Excited state calculation was carried out with the help of TD-DFT method.

Similarly, the ground state geometry optimization was done for β-Bi_2O_3/ $Bi_2O_2CO_3$, the bismuth oxycarbonate (BOC) cluster, PATP and the PATP–BOC system without any constraint on geometry. Vibrational frequencies were computed for the global minimum structure. The SERS spectrum of the PATP–BOC system was also simulated.

TDOS (Total density of states) calculation was performed utilizing multiwfn software to gain insights about the band gap. Molecular electrostatic potential mapping was carried out on the optimized geometry of both systems to visualize the charge density distribution. For the calculation of charge value on each atom of the systems MK (Merz-Kollman) [ESP] charge was calculated. For all the calculation, the generalized gradient approximation (GGA) for exchange–correlation functionals PW91PW91 was used and Cu and Bi atoms were treated by relativistic effective core potentials (RECP) with (LANL2DZ)[29] and for C, H, N, and S atoms 6–311+G(d,p) basis set was used. Calculations were also performed with B3LYP functional but the predictions using the PW91PW91 functional were found to be in significantly good agreement with the experimental results and hence this functional was preferred to B3LYP throughout the study reported herein. Literature is replete with computational predictions where for transition metal elements the LANL2DZ basis set was found to be very efficient and the Pople basis set, 6–311+G(d,p), for organic molecules. For all the calculation Gaussian 16 suite of program was utilized. And the calculated Raman active vibrational modes were assigned on the basis of results of the Gaussview 6.0.16 version.

6.3 Results and discussion

6.3.1 Geometry optimization and simulated SERS spectrum of PATP/DMAB on the copper cluster

All optimized structures did not show any imaginary frequency indicating that they belong to the minimum region in the potential energy landscape and are not transition states. The optimized structures and simulated SERS spectrum of both the systems are shown in Fig. 6.1 and Fig. 6.2, respectively. Comparison of the simulated Raman spectrum of both the system with the experimentally observed SERS spectrum of PATP and normal Raman spectrum of PATP are shown in Table 6.1 and Table 6.3.

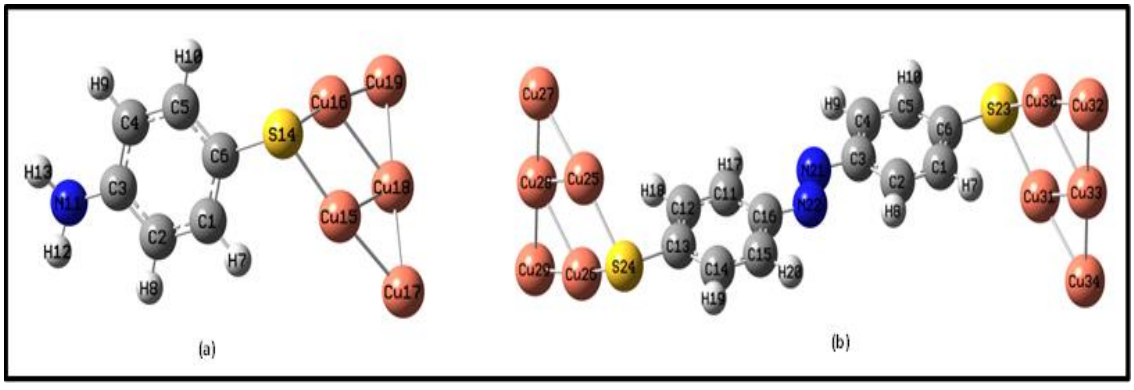

Figure 6.1: Optimized structure of (a) PATP-Cu5 and (b) Cu5-DMAB-Cu5 systems at PW91PW91/LANL2DZ/6–311+G(d,p) level of theory

Table 6.1: Comparison of Raman spectrum of PATP before and after adsorption on Cu5 cluster with Experimental Raman spectrum of solid PATP from literature

Calculated Raman peaks [cm^{-1}] (before adsorption)	**Calculated SERS peaks [cm^{-1}] (after adsorption)**	**Experimental Raman peaks [cm^{-1}] [13]**	**Tentative Assignment#**
367	377		νCS+ γCCC+ δCH
474	488	472	γCCC+ γCH
515	546		ωNH2+ γCH
631	624	639	γCCC+ρNH2
669	709		γCH+δSH
821	819	825	πCH
993	991		αCCC
1082	1072	1090	νCS+δCH
1167	1167	1171	δCH
1283	1277		νCN+ δCH
1482	1476		νCC+δCH
1596	1596	1596	νCC+ ϕNH2
1616	1615		ϕNH2+ νCC
2562		2565	νSH
3097	3086	3060	νCH
3503	3496		νNH

γ = out of plane bending vibration, δ = in plane bending, ρ = rocking vibration, ν = stretching vibration and ϕ = scissoring vibration, π = wagging vibration, α = ring deformation

Table 6.2: Comparison of Simulated SERS of PATP@Cu with previously reported Simulated SERS of PATP@Ag and PATP@Au

Calculated SERS peaks (cm^{-1}) of PATP using Y/LANL2DZ/6-311+G(d,p) level of theory			**Tentative Assignment#**
on Cu cluster (Y=PW91PW91)	**on Ag cluster (Y=B3LYP)[9]**	**on Au cluster (Y=B3LYP)[9]**	
377	377	377	νCS+ γCCC+ δCH
488		491	γCCC+ γCH
546			ωNH2+ γCH
624	634	628	γCCC+ρNH2
709			γCH+δSH
819			πCH
991			αCCC
1072	1071	1074	νCS+δCH
1167	1182	1183	δCH
1277		1280	νCN+ δCH
1476	1491	1492	νCC+δCH
1596	1605	1606	ϕNH2+ νCC
1615			ϕNH2+ νCC

γ = out of plane bending vibration, δ = in plane bending, ρ = rocking vibration, ν = stretching vibration and ϕ = scissoring vibration, π = wagging vibration, α = ring deformation

Table 6.3: Comparison of Experimentally observed SERS of PATP@Cu with simulated Raman (DMAB) and SERS of Cu5-DMAB-Cu5 at PW91PW91/LANL2DZ/6–311+G(d,p) level of theory

Calculated RAMAN peaks of DMAB (cm^{-1}) [before adsorption]	**Calculated SERS of DMAB on Cu cluster (cm^{-1}) [Present work] [after adsorption]**	**Experimental SERS of PATP@Cu (cm^{-1})[13]**	**Calculated SERS of DMAB on Ag cluster (cm^{-1})[9]**	**Calculated SERS of DMAB on Au cluster (cm^{-1})[9]**	**Tentative Assignment#**
481	477		480	474	νCS + δCH
715	709		713	709	αCCC
1082	1064	1080	1068	1058	νCS + δCH
1129	1127	1140	1125	1126	νCN+ δCH
1192	1186		1188	1183	νCN + δCH

1277	1269				δCH
1332	1329				νCC+ δCH
1393	1387	1388	1388	1389	νNN+ νCC
1428	1424	1438	1428	1428	δCH+ νNN
1467	1460			1463	νNN+ δCH
1586	1584	1584	1582	1583	νCC+ δCH
2613					νSH

ν = stretching vibration, δ = in plane bending vibration, α = ring deformation

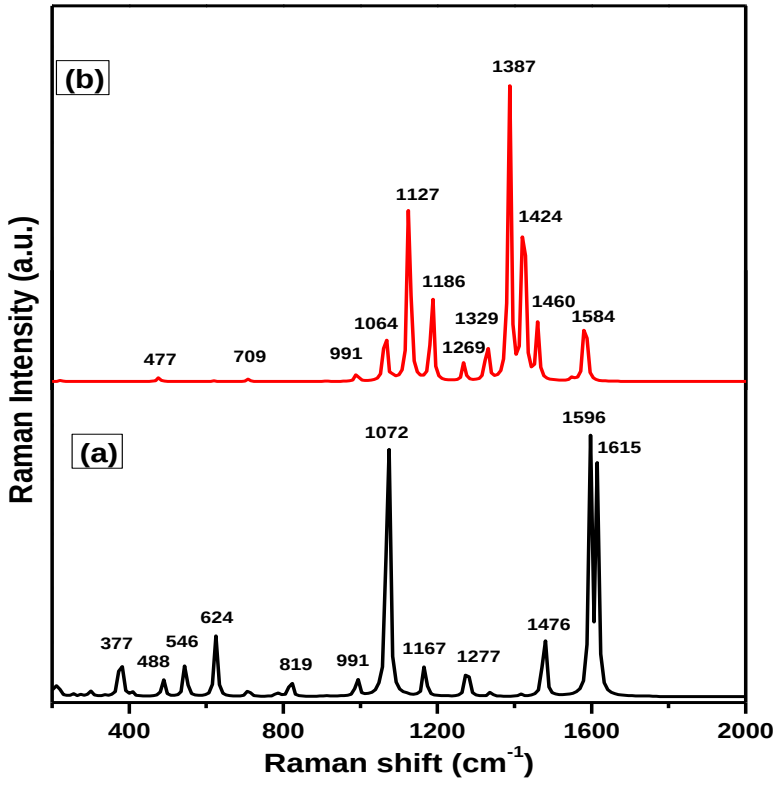

Figure 6.2: Simulated SERS spectrum of (a) PATP-Cu5 and (b) Cu5-DMABCu5 system

The peaks observed at 1090 and 1596 cm^{-1} in the experiment were assigned to the a_1 mode of PATP (Table 6.1) while the peaks at 1171, 1277, 1476 cm^{-1} were assigned to the b_2 mode. It was observed that the peaks of PATP-Cu5 agreed well with the normal Raman spectrum of PATP. Earlier, Wu et al. reported the computational backing to the experimental observation of DMAB in the SERS of PATP using silver and gold cluster.[9] They calculated SERS of PATP on Ag and Au cluster using B3LYP/ LANL2DZ/6–

311+G(d,p) level of theory and used differential scaling factors for various bonds to match their predicted spectrum with the experimental one, albeit only for PATP. In this study also, to confirm the role of copper cluster in the chemical transformation of PATP to DMAB, simulation of SERS was done for both PATP and DMAB. Instead of B3LYP, the PW91PW91 functional was used without scaling for SERS of both PATP and DMAB on copper cluster. Comparing with previous studies (shown in Table 6.2), here too 3 characteristics peaks were observed in case of PATP adsorbed on copper cluster at 1072, 1167, and 1596 cm^{-1} . On the basis of vibrational analysis these bands were attributed to the C–S stretching, C–H in plane bending and the C–C stretching in combination with NH2 scissoring vibration, respectively. The peak at 377 cm^{-1} may be considered as a combination band of C–S stretching, C–C–C bending and C–H in-plane bending vibrations. Though, the peak at 377 cm^{-1} was of very weak in nature. The modes were assigned after visualizing them in Gaussview platform and corroborating with various past studies.[18,30,31] The weak C–S srteching mode in combination with other bending modes observed in the low frequency region has been reported, besides PATP, for 2-ATP and 1,2- benzenedithiol as well.[44] Besides, Wu et al.[18] also assigned these low frequency band as C–S stretching vibration. In the experiment it was observed that the b_2 modes of PATP were enhanced significantly than the a_1 mode but these b_2 modes transformed into a_g modes of DMAB. This observation was confirmed by comparing the simulated Raman of Cu5-DMAB-Cu5 (Fig. 6.2) with the experimentally observed SERS of PATP on copper.

The experimentally observed three intense peaks (1140, 1388 and 1438 cm^{-1}) were in reasonable match with the peaks predicted at 1127, 1387, 1424 in the simulated SERS spectrum of DMAB. The 1127 cm^{-1} arises from the C–N symmetric stretching coupled with C–H in-plane bending vibration. The 1387 cm^{-1} peak has contributions from the N=N stretching coupled with C–C stretching vibrations and the 1424 cm^{-1} is assigned to the N=N stretching coupled with the C–H in-plane bending vibration. It is obvious that these three vibrational modes display very strong Raman signals related to the azo -C–N=N–C functional group. These calculated results too were in good match with the

previous study.[9] The comparison of SERS of DMAB on Ag, Au and Cu cluster is shown in Table 6.3.

The band at 1064 cm^{-1} (a_g type) of DMAB may be correlated to the 1072 cm^{-1} band of PATP (a_1 type) but its intensity in simulated SERS spectrum was very less compared to the N=N stretching band at 1387 and 1424 cm^{-1} which were the significant difference between the two spectra.

Thus the above theoretical vibrational spectroscopic analysis, substantiated the experimental results reported earlier by Arathi et al.[13] very well.

6.3.2 Photon-driven charge transfer (PD-CT) excited state calculations for PATP/DMAB on copper cluster

The relative Raman intensity of the adsorbed molecule is directly influenced by the formation of photon-driven charge transfer (PD-CT) states. Thus to know the PD-CT excited state calculations were carried out using TD-DFT method. In case of PATP-Cu5, the first excited state has an excitation energy 2.00 eV although with a very low oscillator strength of 0.0001 (transition from level 80 to 81 as shown in Fig. 6.3). This excited state arises from the π bonding orbital to the copper 4s antibonding orbital. From Fig. 6.3 shown below, the transition from the level 80 to 82 has relatively larger oscillator strength with excitation energy 2.27 eV where the charge transfer (CT) happens largely from the molecule to metal as well as a small portion from molecule to molecule also ($\pi \rightarrow \pi^*$). In this case also the charge transfer (CT) direction is seen to be on opposite direction of what was reported by Osawa et al. who measured the SERS of PATP on Ag surface.[32] Although the predicted results reported herein are similar to the earlier predictions made for Ag and Au metals.[9]

The CT state from Cu metal to PATP molecule (transition from level 76 to 82) has excitation energy 2.77 eV which is high compared to molecule to metal CT state. Whereas in case of Cu5- DMAB-Cu5 the excited state with large oscillator strength (0.3828) was observed from a mixed excitation of the metal to molecule and $\pi \rightarrow \pi^*$ transition in DMAB itself. And the excitation energy was calculated to be 2.13 eV. This

analysis indicates that the metal to molecule CT is more difficult in PATP-Cu5 while it is more feasible in Cu5-DMAB-Cu5. The molecular orbital plots of PATP and DMAB interaction with copper cluster involved in Photon-driven charge transfer processes are shown in Fig. 6.3.

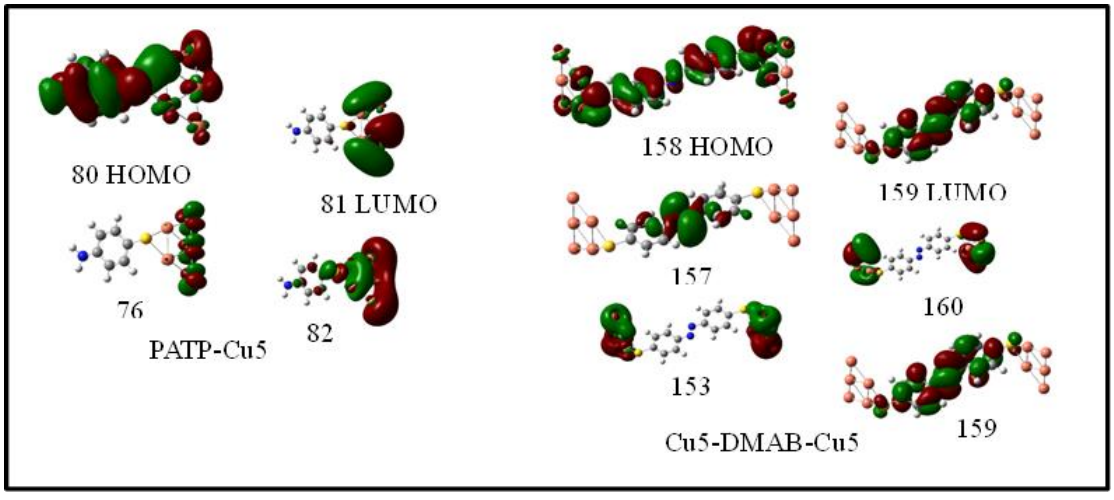

Figure 6.3: Molecular orbital plots of PATP and DMAB adsorbed on copper cluster involved in photon-driven CT processes

6.3.3 Geometry optimization and simulated SERS spectrum of PATP on the bismuth oxycarbonate (BOC) cluster

BOC cluster was modeled and optimized at the PW91PW91/ LANL2DZ/6-311+G(d,P) level of theory (Fig. 6.4). Then PATP and the system containing both PATP and the BOC cluster were optimized at the same level of theory, i.e. PW91PW91/LANL2DZ/ 6-311+G(d,P), as shown in Fig. 6.4c. The interaction energy for the PATP–BOC system was observed to be -54.87 kcal mol^{-1} after subjecting it to BSSE correction, suggesting a strong interaction between the BOC cluster and PATP molecule. Table 6.4 compares the experimental and simulated SERS of PATP. In the simulated SERS spectrum of PATP, the peaks at 1070 cm^{-1} and 1591 cm^{-1} are attributed to the a_1 modes of PATP and found to be in good agreement with the experimentally observed SERS peaks (at 1079 cm^{-1} and 1590 cm^{-1}).

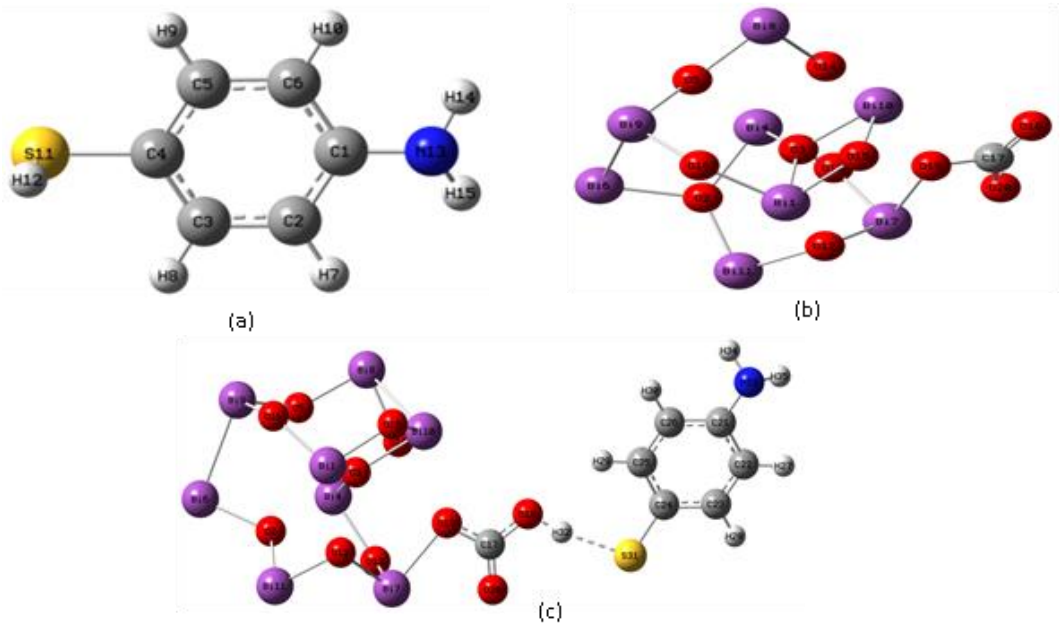

Figure 6.4: Optimized structures; (a) PATP, (b) BOC cluster and (c) PATP-BOC system [the numbers after atom represent the label of respective atom]

Table 6.4: Comparison of the calculated and experimental SERS vibrational frequencies of PATP on the BOC cluster at the PW91PW91/LANL2DZ/ 6-311+G(d,p) level of theory

Experimental SERS peaks of PATP on BOC nanoparticles (cm^{-1})	**Calculated SERS peaks of PATP on BOC cluster (cm^{-1})**	**Tentative Assignment[##]**
630	632	γCCC
822	817	πCH
-	991	Benzene deformation
1079	1070	νCS
1174	1157	δCH
-	1224	νCN+ δCH
1482	1458	νCC+ γCH
1590	1591	νCC

γ = bending vibration, ν = stretching vibration, δ = bending vibration, π = vibration

6.3.4 FMO (frontier molecular orbital) analysis of PATP@BOC

To have an insight about stability and chemical reactivity, FMO calculations have been found to be very efficient. Here, for the calculation of the HOMO–LUMO gap, the ground state properties of PATP–BOC were used. The HOMO is considered as the electron donor, while the LUMO is considered as the electron acceptor. Therefore, to know how the reactivity of PATP changes upon interaction with the BOC cluster through the change in its HOMO–LUMO gap, the FMO calculation was performed at the PW91PW91/LANL2DZ/6-311+G(d,P) level of theory. It can be seen from Fig. 6.5 that, before interaction with the cluster, the HOMO–LUMO gap of PATP was very large, whereas it was significantly reduced in the PATP–BOC system, indicating the increased reactivity of PATP after interaction with the cluster. These observations are confirmed by the total density of states (TDOS) plot (Fig. 6.7) for the BOC cluster before and after the adsorption of PATP on it.

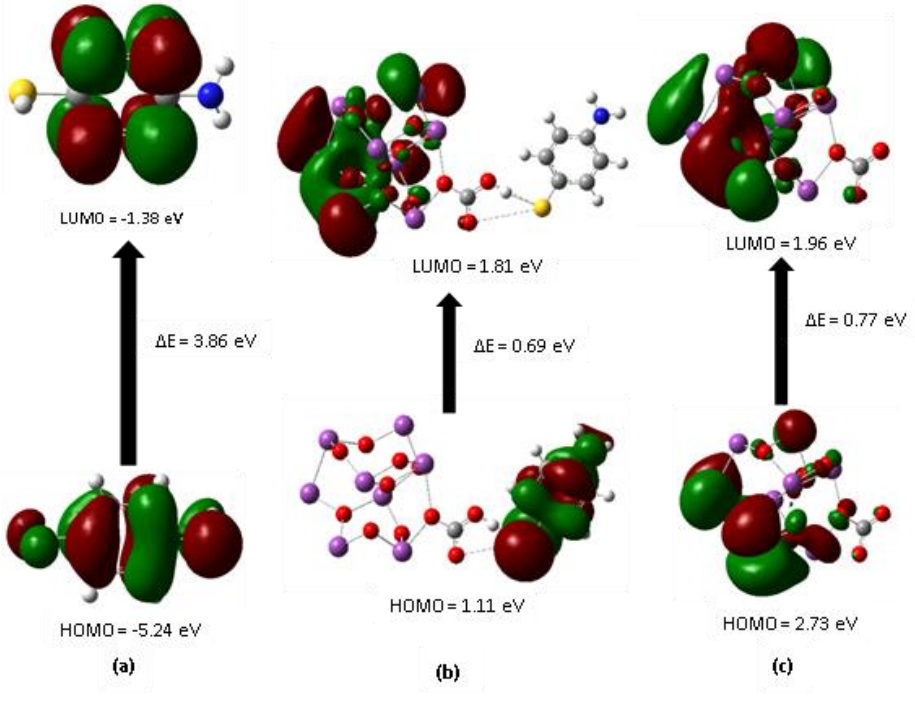

Figure 6.5: Frontier Molecular Orbital diagrams of: (a) HOMO-LUMO of PATP (b) HOMO-LUMO of PATP-BOC system and (c) HOMO-LUMO of BOC cluster

6.3.5a TDOS (total density of states) analysis of PATP/DMAB @ Cu5 cluster

The ground state HOMO (highest occupied molecular orbital)-LUMO (lowest unoccupied molecular orbital) gap and the contribution of atoms in HOMO and LUMO of the PATP-Cu5 and Cu5-DMAB-Cu5 systems was calculated using the TDOS (total density of states) method. The reduced band gap in case of Cu5-DMAB-Cu5 than PATP-Cu5 complex from the TDOS plot shown in Fig. 6.6 suggests a strong interaction between DMAB and copper cluster which provides the stability to this system. From the analysis of the projected density of states (PDOS) it was observed that in the HOMO of the PATP-Cu5 the contribution of PATP is about 65% while Cu5 contribution is about 35%. Similarly, LUMO of PATP-Cu5 consists of 96% contribution from Cu5 while 4% contribution from PATP molecule. It means 61% electron density is transferred from PATP to Cu5 cluster during the transition from HOMO to LUMO of the PATP-Cu5 system. While in case of Cu5-DMAB-Cu5 a reverse trend was observed. Where, in the HOMO the contribution of DMAB is about 63% and Cu cluster contribution is about 37%. And in the LUMO of Cu5-DMAB-Cu5 system the contribution from DMAB is about 95% and from copper cluster the contribution is about 5%. Therefore, unlike to PATP-Cu5 system here 32% electron density is transferred from Cu metal cluster to DMAB molecule during the transition from HOMO to LUMO of the Cu5-DMAB-Cu5 system. These Charge transfer observations in both the systems agree significantly with the previously reported theoretical study[9] where the adsorption of the same molecules was studied on silver and gold instead of copper cluster.

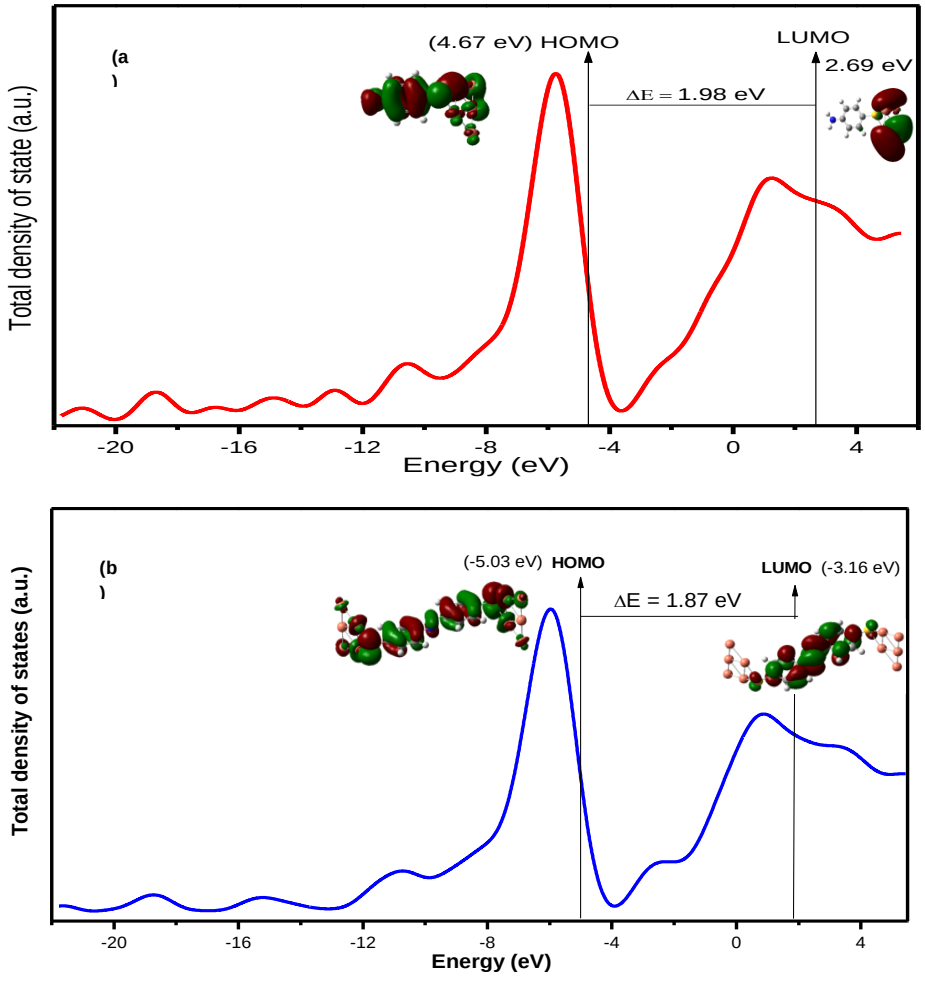

Figure 6.6: TDOS plot for (a) PATP-Cu5 and (b) Cu5-DMAB-Cu5 systems at PW91PW91/LANL2DZ/6-311+G(d,p) level of theory

6.3.5b TDOS (total density of states) analysis of PATp @ BOC

From the TDOS plot shown in Fig. 6.7, it can be said that the energy band gap of the BOC cluster was reduced after interacting with PATP from 0.77 eV to 0.69 eV. This reduced band gap, besides indicating a stronger interaction between the cluster and PATP, confirms the transfer of electron density from PATP to the BOC cluster. From the analysis of the projected density of states (PDOS) it was observed that in the HOMO of the PATP–BOC system the contribution of PATP is about 99.5%, while the BOC cluster contribution is about 0.5%. Similarly, the LUMO of the PATP–BOC system consists of 100% contribution from the BOC cluster and 0% contribution from the PATP molecule.

This means 99.5% electron density is transferred from PATP to the BOC cluster during the transition from the HOMO to the LUMO of the PATP–BOC system. Thus, here, in the case of the BOC cluster there is a molecule to metal charge transfer and this may be the reason for the genuine SERS spectrum of PATP observed experimentally.

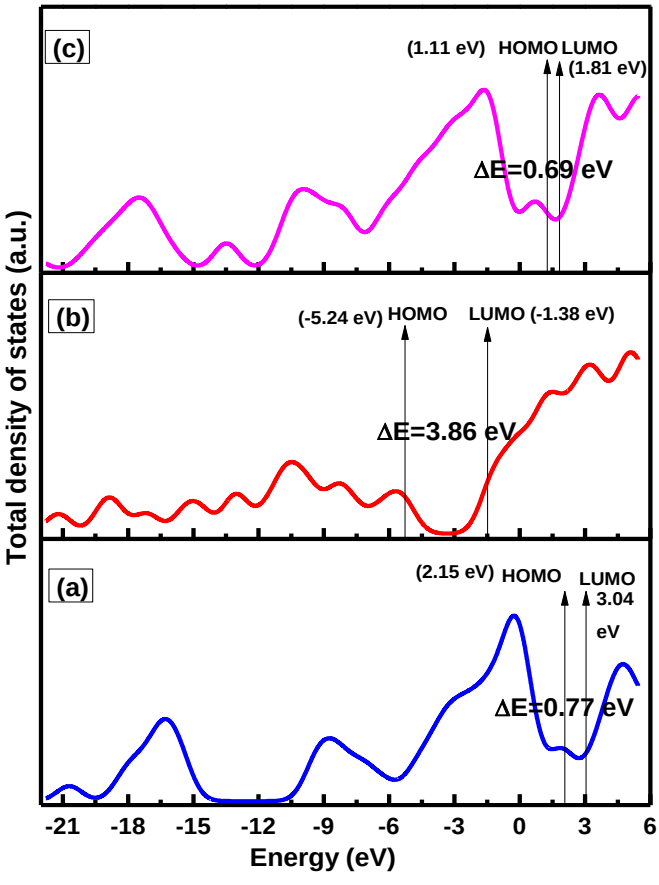

Figure 6.7: Total density of plot of (a) BOC (Bismuthoxycarbonate) cluster (b) PATP and (c) PATP-BOC system showing energy of HOMO, LUMO and band gap (ΔE)

6.3.6 Electrostatic potential maps (MEPs) of PATP/DMAB @ Cu5 cluster

To visualize the possible reactive sites whether electrophilic or nucleophilic and the charge density distribution the molecular electrostatic potential mapping was done on the optimized structures of both systems (PATP/DMAB @ Cu5 cluster). The blue color represents the positive electrostatic potential surface which refers to the lower electron density regions while the red color represents the negative electrostatic potential surface

refers to more electron density regions respectively. Fig. 6.8 shows the ESP map on the optimized structures of PATP-Cu5 and Cu5-DMAB-Cu5 systems. It can be inferred from Fig. 6.8(a) that there is more electron density around sulfur atom and less positive electrostatic potential around Cu cluster which suggests, the interaction between sulfur moiety of PATP and copper cluster occurs via charge density transfer from sulfur to copper cluster. Whereas, in case of Fig. 6.8(b) the electron density around sulfur atoms is more than (a) while there is very less electron density i.e. very high positive electrostatic potential around Cu cluster in (b) comparatively. Thus the ESP map shown in (b) indicates the negative charge density being transferred from copper cluster to DMAB molecule. These observations from ESP mapping reinforced the results obtained from DOS calculations.

ESP [MK(Merz-Kollman)] charges were calculated in order to know the exact charge value on each atom for both the systems (PATP/DMAB @ Cu5 cluster). From the ESP[MK] charges it was observed that the sulfur atom acquired more negative charge in Cu5-DMAB-Cu5 than in PATP-Cu5. Similarly, copper atoms had more positive charges in Cu5-DMAB-Cu5 than in PATP-Cu5, as shown in Table 6.5. This observation also supports the DOS results where charge transfer occurred from molecule to metal in PATP-Cu5 and metal to molecule in Cu5-DMAB-Cu5 due to which these differences in charges on sulfur as well as on copper atoms were observed.

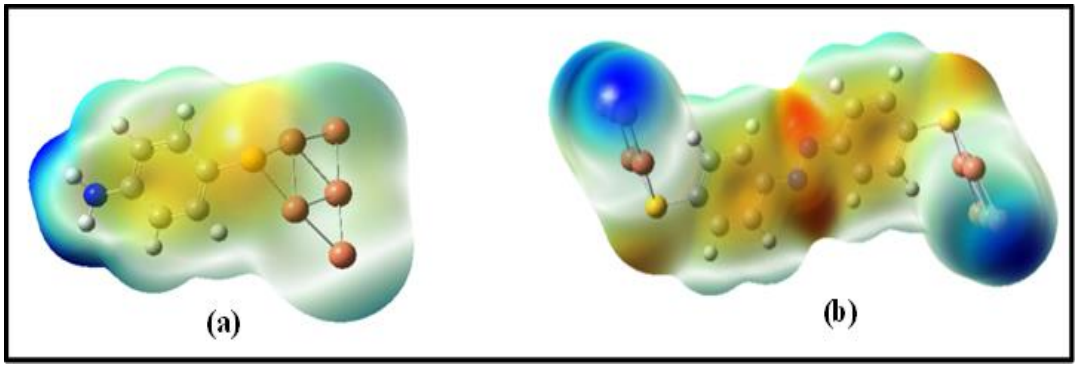

Figure 6.8: ESP map on optimized structures of (a) PATP-Cu5 and (b) Cu5-DMAB-Cu5

Table 6.5: ESP[MK] charge values (a.u.) calculated for Cu5-DMAB-Cu5 and PATP-Cu5 system at PW91PW91/LANL2DZ/6–311+G(d,p) level of theory

Cu5-DMAB-Cu5		**PATP-Cu5**	
Atoms	**Charge (a.u.)**	**Atoms**	**Charge (a.u.)**
C1	0.006	C1	-0.004
C2	0.015	C2	0.012
C3	0.009	C3	0.011
C4	-0.006	C4	-0.005
C5	-0.028	C5	-0.021
C6	-0.023	C6	-0.020
H7	0.018	H7	-0.003
H8	0.026	H8	0.024
H9	-0.002	H9	-0.006
H10	-0.050	H10	-0.034
C11	0.015	N11	0.028
C12	0.005	H12	0.033
C13	-0.023	H13	0.021
C14	-0.028	S14	-0.043
C15	-0.006	Cu15	-0.023
C16	0.009	Cu16	-0.009
H17	0.025	Cu17	0.0005
H18	0.018	Cu18	0.013
H19	-0.051	Cu19	0.025
H20	-0.002		
N21	0.015		
N22	0.015		
S23	-0.057		
S24	-0.057		
Cu25	-0.018		
Cu26	-0.019		
Cu27	0.040		
Cu28	0.035		
Cu29	0.039		
Cu30	-0.018		
Cu31	-0.018		
Cu32	0.040		
Cu33	0.035		
Cu34	0.039		

number after atoms represents the label of that atom in optimized structures shown in figure 6.1.

6.4 Conclusion

It was experimentally known that similar to silver and gold nano-particles, copper nanoparticles also act as a photocatalyst for the chemical transformation of PATP to DMAB. This experimental observation was further supported in present computational study. comparing the simulated Raman spectrum of both PATP and DMAB molecules on the copper cluster with the experimentally observed SERS spectrum of PATP on copper it is concluded that the enhanced b_2 modes of PATP in reality are the a_g modes of DMAB. Thus choice of the level of theory namely, PW91PW91 functional and Cu atoms treated by relativistic effective core potentials (RECP) with (LANL2DZ) and for C, H, N, and S atoms 6–311+G(d,p) basis set may be used for future predictions as the results matched exceedingly well with the experiment. Excited state calculations revealed that photon-driven charge transfer occurred form molecule to metal in PATP-Cu5 while from metal to molecule in Cu5-DMAB-Cu5 which further reinforced that enhanced peaks are not due to PATP but due to its azodimer, DMAB. The low band gap of Cu5- DMAB-Cu5 than PATP-Cu5 suggests higher stability of the system. Also the charge transfer direction were found opposite in both systems where, it was molecule to metal charge transfer in PATP-Cu5 while it was metal to molecule in Cu5-DMAB-Cu5. Molecular electrostatic potential map and MK[ESP] charges further suggest the electron density was transferred from copper to molecule as there is more negative charge on sulfur atoms in Cu5-DMAB-Cu5 system respectively. Thus it can be inferred from this study that copper behaved similar to silver and gold in the surface dimerization reaction of PATP molecule and the reason behind enhanced a_g mode of DMAB on copper is metal to molecule charge transfer along with more stability of Cu5-DMAB-Cu5 system. PW91PW91/LANL2DZ/6–311+G(d,p) level of theory may be considered most accurate to study such systems in future.

Whereas, in case of non-noble metal cluster that is bismuth based cluster (BOC) since the genuine SERS spectrum of PATP was observed in which the peaks of DMAB at 1140, 1390 and 1432 cm^{-1} were absent. This is in contrast to the case of noble metal SERS substrates. Therefore DFT calculations were carried out and have been found very helpful

in gaining an insight into the interaction between PATP and the BOC cluster. An interaction energy of -54.87 kcal/mol suggests the strong interaction between these moieties. FMO analysis revealed the stability of this (PATP@BOC) system. Also from the analysis of the projected density of states it can be inferred that there is charge transfer from the PATP molecule to the BOC cluster which further supports the experimentally observed chemical enhancement effect. The simulated SERS spectrum of PATP@BOC is in good agreement with the currently reported experimental SERS spectrum. Thus this study validates the experimental observation where the genuine SERS spectrum of PATP can be obtained using β-Bi_2O_3/$Bi_2O_2CO_3$ nanoparticles. Moreover, these nanoparticles can also be taken into consideration in the future to obtain the genuine SERS spectra of other molecules where there is a possibility for dimerization.

6.5 References

(1) Zhou, P.; Tian, F.; Lv, F.; Shang, Z. Geometric Characteristics of Hydrogen Bonds Involving Sulfur Atoms in Proteins. *Proteins Struct. Funct. Bioinforma.* **2009**, *76* (1), 151–163.

(2) Huang, Y.-F.; Zhu, H.-P.; Liu, G.-K.; Wu, D.-Y.; Ren, B.; Tian, Z.-Q. When the Signal Is Not from the Original Molecule to Be Detected: Chemical Transformation of Para-Aminothiophenol on Ag during the SERS Measurement. *J. Am. Chem. Soc.* **2010**, *132* (27), 9244–9246.

(3) Amrolia, P.; Sullivan, S. G.; Stern, A.; Munday, R. Toxicity of Aromatic Thiols in the Human Red Blood Cell. *J. Appl. Toxicol.* **1989**, *9* (2), 113–118.

(4) Zhang, L.; Weng, Y.; Liu, X.; Gu, W.; Zhang, X.; Han, L. Fe (III) Mixed IP6@ Au NPs with Enhanced SERS Activity for Detection of 4-ATP. *Sci. Rep.* **2020**, *10* (1), 5752.

(5) Oldenburg, S. J.; Averitt, R. D.; Westcott, S. L.; Halas, N. J. Nanoengineering of Optical Resonances. *Chem. Phys. Lett.* **1998**, *288*, 243–247.

(6) Jiao, L.; Niu, L.; Shen, J.; You, T.; Dong, S.; Ivaska, A. Simple Azo Derivatization on 4-Aminothiophenol/Au Monolayer. *Electrochem. Commun.* **2005**, *7* (2), 219–222.

(7) Sun, M.; Xu, H. Direct Visualization of the Chemical Mechanism in SERRS of 4-Aminothiophenol/Metal Complexes and Metal/4-Aminothiophenol/Metal Junctions. *ChemPhysChem* **2009**, *10* (2), 392–399.

(8) Wu, D.-Y.; Liu, X.-M.; Huang, Y.-F.; Ren, B.; Xu, X.; Tian, Z.-Q. Surface Catalytic Coupling Reaction of P-Mercaptoaniline Linking to Silver Nanostructures Responsible for Abnormal SERS Enhancement: A DFT Study. *J. Phys. Chem. C* **2009**, *113* (42), 18212–18222.

(9) Wu, D.-Y.; Zhao, L.-B.; Liu, X.-M.; Huang, R.; Huang, Y.-F.; Ren, B.; Tian, Z.-Q. Photon-Driven Charge Transfer and Photocatalysis of p-Aminothiophenol in Metal Nanogaps: A DFT Study of SERS. *Chem. Commun.* **2011**, *47* (9), 2520–2522.

(10) Zhao, L.-B.; Huang, R.; Huang, Y.-F.; Wu, D.-Y.; Ren, B.; Tian, Z.-Q. Photon-Driven Charge Transfer and Herzberg-Teller Vibronic Coupling Mechanism in Surface-Enhanced Raman Scattering of p-Aminothiophenol Adsorbed on Coinage Metal Surfaces: A Density Functional Theory Study. *J. Chem. Phys.* **2011**, *135* (13).

(11) Huang, Y.-F.; Wu, D.-Y.; Zhu, H.-P.; Zhao, L.-B.; Liu, G.-K.; Ren, B.; Tian, Z.-Q. Surface-Enhanced Raman Spectroscopic Study of p-Aminothiophenol. *Phys. Chem. Chem. Phys.* **2012**, *14* (24), 8485–8497.

(12) Choi, S.; Jeong, H.; Choi, K.; Song, J. Y.; Kim, J. Electrodeposition of Triangular Pd Rod Nanostructures and Their Electrocatalytic and SERS Activities. *ACS Appl. Mater. Interfaces* **2014**, *6* (4), 3002–3007.

(13) Arathi, P.; Bhaskar, S.; Ramanathan, V.; others. The Photocatalytic Role of Electrodeposited Copper on Pencil Graphite. *Phys. Chem. Chem. Phys.* **2018**, *20* (5), 3430–3432.

(14) Liu, Y.; Li, H.; Shu, W.; Chen, Q. Synthesis and Application of Antimony Pent (Isooctyl Thioglycollate). *J. Cent. South Univ. Technol.* **2005**, *12*, 64–67.

(15) Fang, Y.; Li, Y.; Xu, H.; Sun, M. Ascertaining p, P′-Dimercaptoazobenzene Produced from p-Aminothiophenol by Selective Catalytic Coupling Reaction on Silver Nanoparticles. *Langmuir* **2010**, *26* (11), 7737–7746.

(16) Canpean, V.; Iosin, M.; Astilean, S. Disentangling SERS Signals from Two Molecular Species: A New Evidence for the Production of p, P′-Dimercaptoazobenzene by Catalytic Coupling Reaction of p-Aminothiophenol on Metallic Nanostructures. *Chem. Phys. Lett.* **2010**, *500* (4–6), 277–282.

(17) Zong, S.; Wang, Z.; Yang, J.; Cui, Y. Intracellular pH Sensing Using P-Aminothiophenol Functionalized Gold Nanorods with Low Cytotoxicity. *Anal. Chem.* **2011**, *83* (11), 4178–4183.

(18) Maniu, D.; Chis, V.; Baia, M.; Toderas, F.; Astilean, S. Density Functional Theory Investigation of P-Aminothiophenol Molecules Adsorbed on Gold Nanoparticles. *J. Optoelectron. Adv. Mater.* **2007**, *9* (3), 733.

(19) Wang, Y.; Zhao, H.; Cao, E.; Sun, Y.; Ye, H.; Lin, W.; Wang, R. Pt-Based Nanostructures for Observing Genuine SERS Spectra of p-Aminothiophenol (PATP) Molecules. *Appl. Sci.* **2017**, *7* (9), 953.

(20) Saroj, A.; Sharma, U.; Das, S.; Ramanathan, V. Bismuth Based Novel Substrate for Surface Enhanced Raman Spectroscopy. *Spectrochim. Acta. A. Mol. Biomol. Spectrosc.* **2022**, *280*, 121576.

(21) Shahbazi, M.-A.; Faghfouri, L.; Ferreira, M. P.; Figueiredo, P.; Maleki, H.; Sefat, F.; Hirvonen, J.; Santos, H. A. The Versatile Biomedical Applications of Bismuth-Based Nanoparticles and Composites: Therapeutic, Diagnostic, Biosensing, and Regenerative Properties. *Chem. Soc. Rev.* **2020**, *49* (4), 1253–1321.

(22) Selvamani, T.; Anandan, S.; Granone, L.; Bahnemann, D. W.; Ashokkumar, M. Phase-Controlled Synthesis of Bismuth Oxide Polymorphs for Photocatalytic Applications. *Mater. Chem. Front.* **2018**, *2* (9), 1664–1673.

(23) Foresman, J. Frisch E.(1993). Exploring Chemistry with Electronic Structure Methods, Gaussian. *Inc Pittsburgh*.

(24) Wu, D.; Hayashi, M.; Shiu, Y.; Liang, K.; Chang, C.; Yeh, Y.; Lin, S. A Quantum Chemical Study of Bonding Interaction, Vibrational Frequencies, Force Constants,

and Vibrational Coupling of Pyridine- M n (M= Cu, Ag, Au; N= 2- 4). *J. Phys. Chem. A* **2003**, *107* (45), 9658–9667.

(25) Muniz-Miranda, M.; Muniz-Miranda, F.; Caporali, S. SERS and DFT Study of Copper Surfaces Coated with Corrosion Inhibitor. *Beilstein J. Nanotechnol.* **2014**, *5* (1), 2489–2497.

(26) Ferral, A.; Paredes-Olivera, P.; Macagno, V.; Patrito, E. Chemisorption and Physisorption of Alkanethiols on Cu (111). A Quantum Mechanical Investigation. *Surf. Sci.* **2003**, *525* (1–3), 85–99.

(27) Ahmed, A. A. Structural and Electronic Properties of the Adsorption of Nitric Oxide Molecule on Copper Clusters CuN (N= 1–7): A DFT Study. *Chem. Phys. Lett.* **2020**, *753*, 137543.

(28) Crispin, X.; Bureau, C.; Geskin, V.; Lazzaroni, R.; Brédas, J.-L. Local Density Functional Study of Copper Clusters: A Comparison between Real Clusters, Model Surface Clusters, and the Actual Metal Surface. *Eur. J. Inorg. Chem.* **1999**, *1999* (2), 349–360.

(29) Hay, P. J.; Wadt, W. R. Ab Initio Effective Core Potentials for Molecular Calculations. Potentials for the Transition Metal Atoms Sc to Hg. *J. Chem. Phys.* **1985**, *82* (1), 270–283.

(30) Madzharova, F.; Heiner, Z.; Kneipp, J. Surface-Enhanced Hyper Raman Spectra of Aromatic Thiols on Gold and Silver Nanoparticles. *J. Phys. Chem. C* **2020**, *124* (11), 6233–6241.

(31) Griffith, W. P.; Koh, T. Y. Vibrational Spectra of 1,2-Benzenedithiol, 2-Aminothiophenol and 2-Aminophenol and Their SER Spectra. *Spectrochimica Acta Part A: Molecular and Biomolecular Spectroscopy*, 1995, *51*, 253–267. https://doi.org/10.1016/0584-8539(94)E0086-P.

(32) Osawa, M.; Matsuda, N.; Yoshii, K.; Uchida, I. Charge Transfer Resonance Raman Process in Surface-Enhanced Raman Scattering from p-Aminothiophenol Adsorbed on Silver: Herzberg-Teller Contribution. *J. Phys. Chem.* **1994**, *98* (48), 12702–12707.